The Southern Ocean Waves Experiment. Part I: Overview and Mean Results

MICHAEL L. BANNER AND WEI CHEN

The University of New South Wales, Sydney, Australia

EDWARD J. WALSH*

NASA/Goddard Laboratory for Hydrospheric Processes, Observational Science Branch, Wallops Island, Virginia

JORGEN B. JENSEN AND SUNHEE LEE

CSIRO Atmospheric Research, Mordialloc, Victoria, Australia

CHRIS FANDRY+

CSIRO Marine Laboratories, Hobart, Tasmania, Australia

(Manuscript received 24 February 1998, in final form 27 July 1998)

ABSTRACT

The Southern Ocean Waves Experiment (SOWEX) was an international collaborative air–sea interaction experiment in which a specially instrumented meteorological research aircraft simultaneously gathered atmospheric turbulence data in the marine boundary layer and sea surface topography data over the Southern Ocean for a wide range of wind speeds. The aim was to increase present knowledge of severe sea state air–sea interaction. This first paper presents an overview of the experiment and a detailed discussion of the methodology and mean results. A companion paper describes the findings on variability of the wind speed and wind stress and their relationship to variations in the underlying sea surface roughness.

1. Introduction

As the dominant driving source for the surface layer of the world's oceans, the sea surface wind stress τ represents a complex interfacial momentum exchange process between the wind and the underlying wind waves and surface currents. Until fairly recently, in most modeling applications the wind stress has been taken to be a prescribed function only of the reference wind speed alone (usually determined 10 m above the mean sea surface and denoted by U_{10}). There has been no explicit reference to the sea state even though wind waves are a conspicuous feature of the wind-driven interface. An extensive literature documents previous studies on the challenging task of measuring the wind stress over the open ocean. However, observed wind stress data show a surprisingly large scatter when the equivalent drag coefficient is plotted against the reference mean wind speed. This variability is apparent in Fig. 1 where various parameterizations proposed by several authors are superimposed. Underlying sources of this variability have been reported in detail in Donelan (1990), Geernaert (1990), and more recently by Rieder (1997).

The wind stress plays a central role in modeling various wind-driven air–sea interaction processes including sea state prediction, large-scale ocean circulation, and climate evolution. Accurate parameterization of the wind stress is needed to optimize the reliability of these model predictions; consequently, recent investigations have attempted to better understand the causes of its substantial observed variability. With improvements in instrumentation technology, evidence has been accumulating that the sea state may cause a measurable change in the observed wind stress at a given wind speed and might be responsible for some of the scatter observed in Fig. 1. Other investigations have addressed the potential role of larger-scale organized flows in the

* Current affiliation: NOAA/Environmental Technology, Boulder, Colorado.

+ Current affiliation: Department of Environmental Protection, Perth, Australia.

Corresponding author address: Prof. Michael L. Banner, School of Mathematics, The University of New South Wales, Sydney 2052, Australia.
E-mail: m.banner@unsw.edu.au

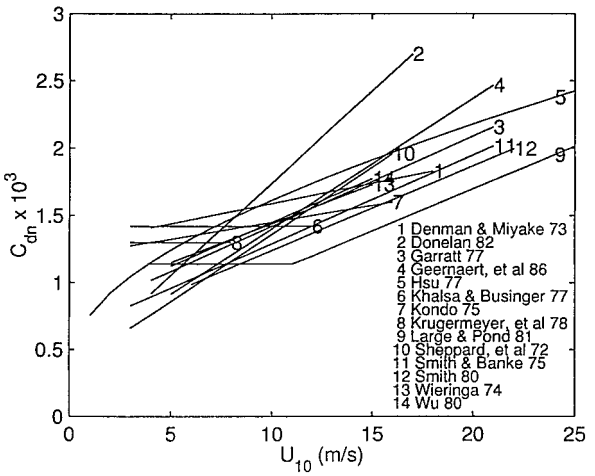

FIG. 1. A historical summary of the scatter among previous determinations of the variation of the neutral sea surface drag coefficient with U_{10}.

atmosphere, such as atmospheric roll cells. An assessment of such influences was a primary motivation for this study.

Historically, the wind stress has proven to be an elusive quantity to measure reliably. Measuring it directly at the sea surface is not feasible, so it needs to be inferred from wind measurements above the sea surface. These measurements have been primarily from fixed towers, with a smaller number from ships and low-flying aircraft. The most direct approach, known as the eddy correlation technique, involves measuring the directional components of the near-surface turbulent stress covariance (defined in section 3) in the atmospheric boundary layer. The data must be measured over sufficiently large time and space scales to capture all scales of variability, which can present significant logistical difficulties. Chen et al. (1999, manuscript submitted to *J. Phys. Oceanogr.*, hereafter referred to as Part II) discuss this aspect for the conditions encountered during the Southern Ocean Waves Experiment (SOWEX).

An alternative technique for quantifying the magnitude of the wind stress developed from the form of wind profile over land. In this approach, based on equilibrium turbulent boundary layer modeling, the vertical wind profile is taken to have the form

$$U(z) = \frac{u_*}{\kappa}\left[\ln\left(\frac{z}{z_0}\right) - \psi_m(z/L)\right]. \tag{1}$$

Here $U(z)$ is the wind speed at height z meters above ground level, u_* is the surface wind friction velocity given by $(\tau/\rho_a)^{1/2}$ (ρ_a is the air density), z_0 is the aerodynamic roughness length, and $\kappa = 0.4$ is the von Kármán constant. Also, following Paulson (1970), ψ_m is the thermal stratification function given for unstable conditions ($z/L < 0$) by

$$\psi_m(z/L) = \ln\left[\left(\frac{1+x^2}{2}\right)\left(\frac{1+x}{2}\right)^2\right] - 2\arctan x + \frac{\pi}{2}, \tag{2a}$$

where $x = (1 - 16z/L)^{1/4}$ and for stable conditions ($z/L > 0$) by

$$\psi_m(z/L) = -5\frac{z}{L}. \tag{2b}$$

Here, the Monin–Obukhov stability length L is defined by

$$L = \frac{-T_v u_*^3}{g\kappa\overline{wT_v}}, \tag{3}$$

where T_v is the virtual temperature and g is the gravitational acceleration. An associated drag coefficient is defined as $C_d = u_*^2/U_{10}^2$. For the aerodynamically smooth flow over the sea surface found at low wind speeds (below $\sim$3 m s^{-1}), viscous stresses dominate the momentum flux from the wind to the sea surface, and most authors (e.g., Smith 1980; Large and Pond 1981, among others) parameterize the surface roughness in terms of the friction velocity and the kinematic viscosity of the air (ν) by

$$z_0 = 0.11\nu/u_*. \tag{4}$$

As the winds strengthen, wind seas develop and the wind stress increases, with a growing fraction of the momentum flux to the sea surface occurring as wave form drag. Accordingly, the air flow becomes aerodynamically rougher. In order to parameterize the aerodynamic roughness length z_0, Charnock (1955) proposed that

$$z_0 = \alpha u_*^2/g, \tag{5}$$

where α is known as the Charnock coefficient. For typical well-developed open ocean conditions, Smith (1980, 1988) reported $\alpha = 0.011$, while from compilations of results that included coastal sites with presumably less mature waves, $\alpha = 0.0145$ (Garratt 1977) or 0.018 (Wu 1980).

Over the past few decades, a large number of field determinations of wind profile, wind stress, and sea surface drag coefficient have been made over the ocean from which a statistically significant wind speed dependence of the drag coefficient has been established. This is usually expressed in the form

$$C_d = a + bU_{10}, \tag{6}$$

where the coefficients a and b are determined from experimental data. A selection of such linear regressions is shown in Fig. 1. Many of these observational results for C_d were reviewed by Wu (1980) and Geernaert (1990).

Changes in wave form drag associated with different sea states are one potential source of variability observed in Fig. 1. This was recognized by Stewart (1974),

who argued for a sea state dependence in the drag coefficient and proposed an extension of the Charnock relation in which the roughness length is a function of wave age; that is,

$$z_0 = \frac{u_*^2}{g} f(c_p/u_*), \tag{7}$$

where c_p is the phase speed of the spectral peak waves. However, the first documented evidence of a wave age dependence in C_d was only reported several years later by Donelan (1982), who observed that the drag coefficient over young wind seas was up to 50% larger than the drag coefficient over old wind seas for comparable wind speeds. Geernaert et al. (1987) also reported that the young wind seas observed from a tower at shallower water sites had significantly larger wind stress levels for a given wind speed and proposed a drag coefficient relation involving the wave age of the form $C_d = A(c_p/u_*)^B$, where, disregarding the data when very long swell waves were present, $A \sim 0.0148$ and $B \sim -0.738$. This wave age dependence was also investigated in the HEXMAX experiment (e.g., see Smith et al. 1992) conducted in the North Sea in 18-m water depth. Applying a systematic correction to the wind data for platform distortion, Smith et al. (1992) obtained $f(c_p/u_*) = 0.43(c_p/u_*)^{-0.961}$, suggesting that the drag coefficients for wind seas generated by high winds in coastal and shallow water sites are significantly higher than those observed for open ocean conditions. However, the conclusions from HEXMAX on sea state dependence in C_d are not unqualified (e.g., Janssen 1997; Oost 1997).

Yelland and Taylor (1996) reported an extensive dataset measured in the Southern Ocean for an extremely wide range of wind speeds and sea states. Their results are based on another observational technique for inferring the wind stress magnitude known as the inertial-dissipation method. This technique depends on an assumed dependence on u_* in the spectral level of the inertial subrange of the turbulence spectrum and can be measured conveniently by a shipborne sonic anemometer. One of the key findings of the Yelland and Taylor (1996) study was that, despite the large range of sea states encountered, the influence of sea state on the drag coefficient did not stand out. According to these authors, this is possibly due to the presence of swell in masking the local wind sea. However, the underlying assumptions for the validity of the inertial-dissipation rate method may not be met during the growth of strongly forced, young wind seas nor in the presence of swell, but this is beyond the scope of this paper. The dissipation technique and its potential limitations are discussed in detail in Fairall and Larsen (1986), Edson et al. (1991), and Geernaert (1990). In any event, the present dataset from the SOWEX data allowed an intercomparison of u_* estimates based on the dissipation and the eddy-correlation methods. In a very recent field study, Rieder and Smith (1998) identified strong wave effects on the wind stress vector by suitable filtering of the momentum flux signal.

As a refinement of the Charnock relation (5), Donelan (1990) and Donelan et al. (1993) proposed a sea state dependence for z_0 explicitly involving the rms wave height σ and the inverse wave age U_{10}/c_p in the form

$$\frac{z_0}{\sigma} = A_0 \left(\frac{U_{10}}{c_p}\right)^{B_0}, \tag{8}$$

with $A_0 = 5.53 \times 10^{-4}$ and $B_0 = 2.66$ from field data, while $A_0 = 9.76 \times 10^{-6}$ and $B_0 = 3.48$ from laboratory data. We note that (8) assumes a wind sea in the absence of significant swell. Donelan (1990) investigated (8) for a wide range of laboratory ($5.5 < U_{10}^{\text{equiv}} < 21$ m s^{-1}, $6.5 < U_{10}^{\text{equiv}}/c_p < 21$ m s^{-1}) and neutrally stable field conditions ($5.2 < U_{10} < 17.3$ m s^{-1}, $0.8 < U_{10}/c_p < 4.6$ m s^{-1}). Here U_{10}^{equiv} is the wave tank wind speed extrapolated to the 10-m reference height. Donelan reported a distinct difference between field and laboratory roughness correlations based on (8) that also persisted for both of the alternate choices of reference wind speeds $U_{\lambda/2}$ and u_* in the inverse wave age term, suggesting that the choice of rms wave height as a reference wave height is not optimal. On the other hand, finding a single, *universal* reference wave height roughness parameter proves to be elusive. Here, a detailed understanding of the spectral contribution of different wave scales on the wind stress might contribute a better parameterization of the sea state influence on the wind stress. In this direction, several authors (see Komen et al. 1994, section II.2.7) have recently proposed models that include the form drag contributions from the entire wave spectrum. However, these models have potentially significant uncertainties associated with the behavior of the high wavenumber tail of the wave spectrum and also with the relative importance of tangential stress.

Overall, despite significant progress with the case of pure wind seas, it would appear that a complete understanding is yet to emerge on quantifying the sea state dependence in the drag coefficient, especially when swell is present. The underlying fluid dynamical processes are highly complex and incompletely understood, while the observational data capable of isolating the sea state influence has been scant and possibly influenced by other systematic sources of variability as discussed earlier. The very recent findings reported by Rieder and Smith (1998) may help to clarify some of these issues, but this is beyond the scope of the present paper.

As originally conceived, Charnock's formula (5) describes the surface roughness for fully aerodynamically rough surfaces where the net momentum flux from the atmosphere to the sea surface is due entirely to form drag over the surface roughness elements. However, the extent to which the sea surface is aerodynamically rough has been an open question for several decades (e.g., Phillips 1977; Donelan 1990), with a diverse range of viewpoints prevailing due to the extreme difficulty in measuring reliably any of the stress contributions—normal, tangential, or total. This is a separate issue from

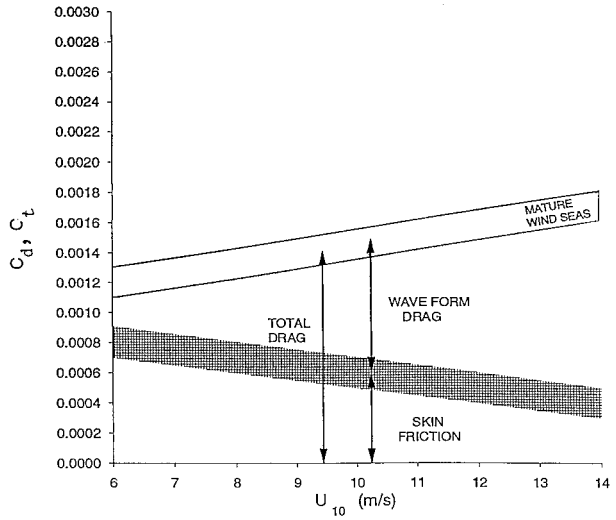

FIG. 2. Variation of the predicted stress partitioning with wind speed U_{10} for mature wind sea conditions according to Banner and Peirson (1998). The upper curve is the familiar wind speed variation of total drag coefficient for mature wind seas. The lower curve is the proposed wind speed variation of the tangential drag coefficient. The difference between these curves gives the wind speed variation of the wave form drag coefficient.

the wave age dependence at a fixed wind speed, which could not be addressed by the SOWEX data. However, in a recent observational study of the wind stress partitioning between form drag and viscous tangential stress, Banner and Peirson (1998) proposed that for wind speeds up to 14 m s^{-1}, the nondimensional aerodynamic roughness length (Charnock coefficient) of the sea surface depends on both wind speed and sea state. These authors related the issue of aerodynamic roughness to the ability of viscous sublayers to reestablish in the presence of wave breaking, particularly at the microscale level. The Banner and Peirson (1998) prediction for the tangential drag coefficient for mature seas under moderate to strong wind speeds is shown in Fig. 2. The key point is that the tangential stress coefficient decreases with wind speed and is relatively insensitive to the sea state. As the overall drag coefficient increases with wind speed, the relative importance of the form drag also increases, resulting in an increasing Charnock coefficient with wind speed. This viewpoint will be reviewed below in the context of the trend of the roughness lengths derived from the SOWEX data and from Yelland and Taylor (1996). For higher wind speeds in the gale force range, we note that other interfacial processes such as wave tearing and the spray layer may also play a significant role in the surface-layer dynamics. These additional mechanisms may require parameterization beyond those underlying the familiar roughness length relationship.

The foregoing discussion raises interesting questions about the physical sea surface roughness that underlies the aerodynamic roughness. From the observational viewpoint, it would appear that the aerodynamic roughness is not well-correlated with the height of the dominant wind waves alone, even with adjustments for the wave age (e.g., Donelan et al. 1993). Conceptually, a more appropriate physical roughness measure should involve the smaller-scale roughness elements that contribute significantly to the wave form drag, yet direct measurement of the *entire* wavenumber spectrum for the wave field is a daunting task and is not presently feasible. However, following the model of Plant (1982), the mean square sea slope (mss) may provide a useful measure of the sea surface roughness that is accessible through available measurement techniques. The directionally integrated mss of the sea surface, s^2, is defined by

$$s^2 = \int_{-\infty}^{\infty}\int_{-\infty}^{\infty} k^2\Phi(\mathbf{k})\, d\mathbf{k}, \tag{9}$$

where $\Phi(\mathbf{k})$ is the directional wavenumber spectrum and $\mathbf{k}$ is the wavenumber vector.

Based on sun glitter photographs of the wind-driven sea surface taken from an aircraft and the wind speed measured from a nearby vessel, Cox and Munk (1954) reported a linear relation between optical bandwidth mss and 12-m height wind speed for $0 < U_{12} < 14$ m s^{-1}:

$$s^2 = 0.003 + 0.00512U_{12}. \tag{10}$$

Since the classical Cox and Munk (1954) results, more recent mss observations have become available from certain active microwave remote sensing techniques. Applying Barrick's model (see below) to their K_u-band (14 GHz) near-nadir radar data using their Radar Ocean Wave Spectrometer (ROWS) instrument, Jackson et al. (1992) proposed the following relation between wind speed and mss from their backscatter data for $7 < U_{10} < 15$ m s^{-1} for a measurement bandwidth out to $O(2$ cm) wavelengths:

$$s^2 = 0.013 + 0.0023U_{10}. \tag{11}$$

More recently, Walsh et al. (1998a,b) measured mss in the western equatorial Pacific Ocean for wind speeds less than 11 m s^{-1}.

Overall, there have been relatively few observations of mss reported in the literature, particularly for the gale force wind regime. However, if such relationships between wind speed and mss are generally valid, that is, hold for different wave age conditions, then a useful relationship between mss and wind stress should be available via the wind speed dependence of the drag coefficient. This possibility is explored in the discussion below. Finally, we note that very recently Anctil and Donelan (1996) proposed an extension of the Donelan (1990) nondimensional roughness length relationship that includes the mss. This relationship has the form

$$\frac{z_0}{\sigma} = 2.26\left(\frac{U_{10}}{c_p}\right)^{1.82}(s^2)^{1.915}. \tag{12}$$

The extent to which the rather limited SOWEX wind sea data fit this relationship is discussed below.

Returning to the issue of uncertainty in reported C_d measurements, we note that despite the substantial observational database, Fig. 1 shows that a large scatter persists in reported drag coefficient data. The known influence of atmospheric stability has been incorporated through the Monin–Obukov stability parameter L (e.g., see Geernaert and Katsaros 1986), and more recent attention has focused strongly on the sea state influence on C_d, as discussed above. Another possible sea state influence was suggested by Geernaert (1991), who proposed that background, large-scale, swell waves traveling obliquely to the local wind may modify the direction of the wind stress vector via hydrodynamic distortion of the directional spectrum of the stress-supporting short wind wave components. Yet another potential source of variability is the influence of larger-scale organized flows in the wind field, such as atmospheric roll vortices that occur frequently in the planetary boundary layer (e.g., see Etling and Brown 1993). However, the potential impact of roll cell structures on the variability of the wind stress does not appear to be widely appreciated. These fundamental issues provided the background and motivation for the present study.

Observations and methodology

To extend existing knowledge on sources of variability of the wind stress, we carried out a comprehensive aircraft measurement program known as the SOWEX. A novel feature of SOWEX was the measurement of mss simultaneously with the large-scale wave topography, wind speed, and atmospheric turbulence measurements in the marine boundary layer. From these data we were able to calculate the mean wind stress, the sea surface drag coefficient, and the associated surface wave properties for the wide range of wind speeds from gale force to quiescent that prevailed during SOWEX. However, the nominal wave age range encountered during the SOWEX mission window did not allow us to address the issue of sea state influence on the wind stress. Nevertheless, we were able to obtain significant insight into the issue of the contributions to the wind stress of different atmospheric turbulence length scales and their impact on its variability.

In this first paper, we describe the SOWEX experiment and the various data analyses undertaken. We report the observed dependence of the overall mean atmospheric fluxes and the mean square slope on the wind speed. Our companion paper (Part II) reports our findings on the variability of the wind speed and the wind stress in relation to the underlying sea surface roughness, as measured by the mss and dominant wave height.

2. The SOWEX experiment

SOWEX was an international, collaborative air–sea interaction experiment conducted by scientists from The University of New South Wales, Australia; CSIRO Atmospheric Research and CSIRO Marine Laboratories, Australia; NASA/Goddard Space Flight Center; and the University of Massachusetts. A major goal of the research was to increase our present understanding of the structure of the sea surface wind stress and its relation to the underlying sea surface roughness.

SOWEX was carried out during 10–16 June 1992 over the Southern Ocean, off the southwest coast of Tasmania, Australia (42°–45°S, 143°–147°E), as shown in Fig. 3. In winter, the wind often blows over the Southern Ocean consistently from the south-southwest, so the ocean fetch can be treated as infinitely long. The weather during the seven days of the experiment evolved from the peak of a storm to a near-calm sea state. Figure 4 gives an indicative summary of the atmospheric and sea state conditions for the month of June 1992 as recorded at Granville Harbour, some 200 km north of the SOWEX site (see Fig. 3). During the SOWEX period, the 10-m mean wind speed decreased from almost 20 m s^{-1} on 10 June to less than 2 m s^{-1} on 16 June. The temperature of the sea surface (11°–13°C) was warmer than the air temperature (~10°C), resulting in unstable thermal stratification.

The sea state during SOWEX

The gale force winds and long fetches encountered during SOWEX (see Fig. 4) produced high wind seas with very long wavelengths (λ). Following Donelan (1990, §4, p. 261), we believe that the use of a wave age based on $U(\lambda/2)$ as reference wind speed rather than U_{10} represents a more self-consistent and physically realistic indicator of the strength of the wind forcing of these waves. For example, during the strongest wind speed day (10 June), the significant wave height (SWH) reached 9.2 m. On this day, according to customary inverse wave age considerations, $U_{10}/c_p \sim 0.9$, and therefore this wind sea was nominally very close to full development. However, the level of whitecap activity at the spectral peak was indicative of younger wind sea behavior and one must question the applicability of the U_{10}/c_p criterion in such large-scale seas. The intrinsic wave age $U(\lambda/2)/c_p$ for this case is 1.2, consistent with appreciable wind coupling to the dominant waves.

Table 1 summarizes the general weather and sea state conditions during SOWEX, including this intrinsic wave age. From this table, it is seen that on 10 and 12 June, $U(\lambda/2)/c_p$ exceeded 1, and we believe that these cases constituted active generation cases of the dominant waves. On 10 June, the SWH, peak period and one-dimensional wavenumber spectral tail shape (see Fig. 11b) are consistent with ''standard'' (e.g., JONSWAP, Hasselmann et al. 1973) wind sea behavior for a mature wind sea with $U_{10} \sim 20$ m s^{-1}. For 11 June, the intrinsic wave age is inconclusive, but the SWH, peak period, and spectral shape indicate that this should not be considered a fully developed wind sea, but rather as swell.

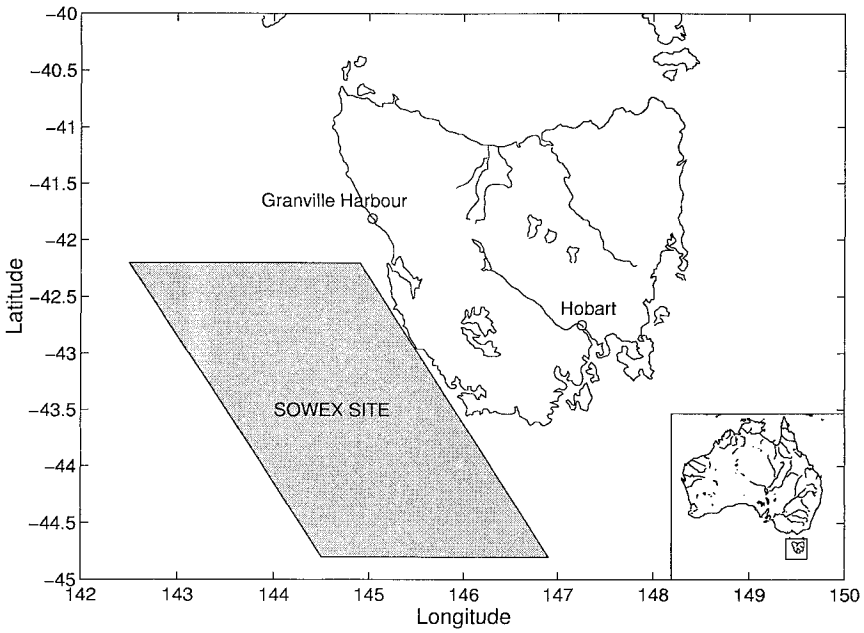

FIG. 3. The SOWEX site off the southwest coast of Tasmania.

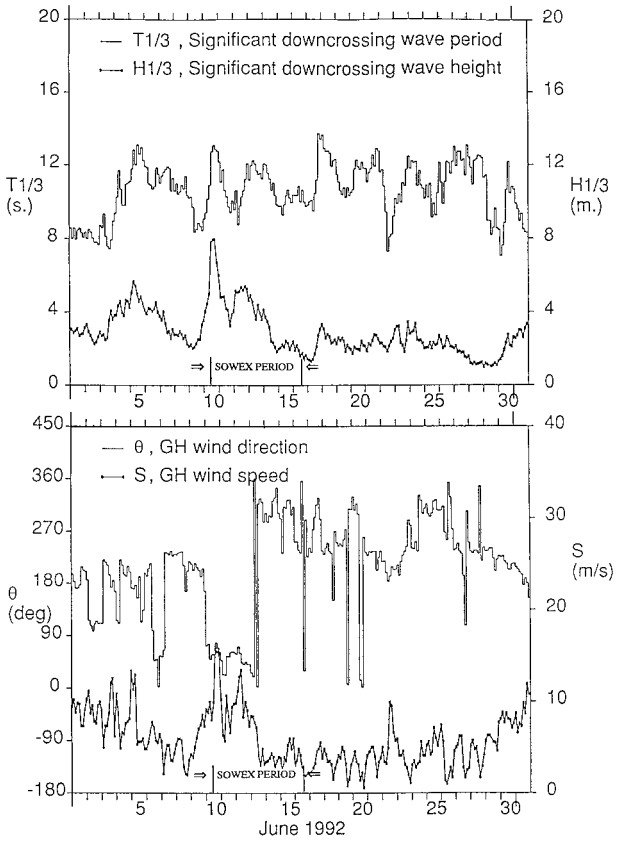

FIG. 4. Wind and wave conditions during June 1992 at Granville Harbour (location shown in relation to the SOWEX site in Fig. 3). The SOWEX observation period is indicated.

On 12 June, despite the evident strong growth and large SWH, the peak period of 13.2 s is lower than that of a wind sea for $U_{10} = 16$ m s^{-1}. Thus, 12 June might be regarded as a complex mix of wind sea and collinear swell rather than as wind sea. The ensuing days with decreasing winds were clearly cases of swell.

SOWEX relied entirely on measurements made from the CSIRO F27 scientific research aircraft, which is 25 m long with a 29-m wing span and has a 6-m measurement nose cone. It was comprehensively equipped to collect atmospheric turbulent flux and sea surface data. Signals from sensors measuring static and dynamic pressure, wet and dry temperatures, and flow angles were filtered using a four-pole, 25-Hz low-pass Butterworth filter and then logged at 64 Hz along with inertial navigation system data. This data was subsequently used for calculating wind speed and direction, the components of the wind stress vector, sensible heat flux, moisture flux, and atmospheric stratification. These meteorological sensors are described fully in Chen (1997). The 36-GHz (8-mm wavelength) NASA Scanning Radar Altimeter (SRA) was installed in the middle section

TABLE 1. Summary of weather and sea state conditions during the SOWEX missions.

Date (June)	U_{10} (m s^{-1})	Dir (deg)	z/L	H_s (m)	T_p (sec)	$U(\lambda/2)c_p$	c_p/μ_*
10	20	239	−0.17	9.2	13.7	1.2	23
11	15	247	−0.15	4.2	12.9	0.9	—
12	16	230	−0.11	6.2	13.2	1.0	30
13	9	201	−0.50	4.0	13.8	0.5	—
14	6	210	−0.65	2.0	13.8	0.4	—
16	<2	200	—	—	9.8	<0.1	—

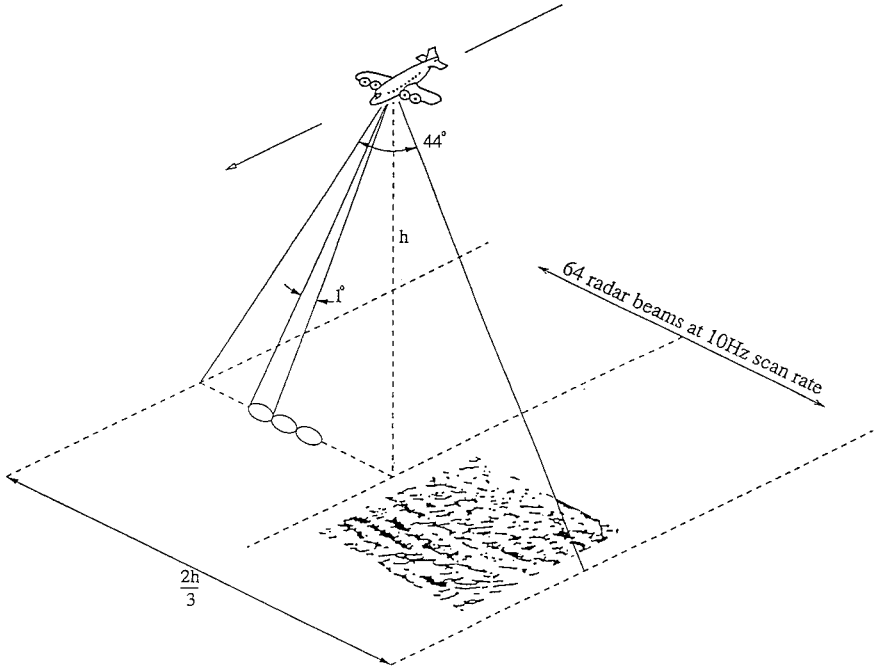

FIG. 5. Schematic of the NASA Scanning Radar Altimeter (SRA).

of the aircraft. The SRA scans its 1° beam at 10 Hz in the cross-track direction from −21.83° to 21.83° with respect to nadir in 0.043 s, producing 64-point raster scan lines of sea surface topography and of backscattered power. A schematic diagram is shown in Fig. 5. The typical aircraft measurement air speed was about 76 m s^{-1} relative to the air mass. Thus, the aircraft ground speed was about 53 m s^{-1} during the upwind flight on 10 June when the wind speed was about 23 m s^{-1}. This gave alongtrack and cross-track sampling intervals of 5.3 and 1 m, respectively, when flying upwind at an altitude of 60 m. These sampling intervals varied with wind speed, flight direction, and altitude, but this typifies the much lower wavenumber resolution available from alongtrack sampling compared with cross-track sampling for these low flying heights. Finally, we note that analysis of the variation of backscattered power data versus incidence angle deviation from nadir yields the mss of the sea surface.

Each of the six observational flight missions comprised

1) a lowest permissible height (H_{min}) flight in a triangular pattern, with one upwind/downwind track and two crosswind tracks,
2) a crosswind direction leg at $2H_{min}$,
3) circle flights for SRA measurements of the azimuthal variation of mss,
4) sounding flights over the entire depth of the marine atmospheric boundary layer (MABL),
5) flight segments for determining directional spectra of the surface waves,
6) flights for instrument calibrations.

In (1) and (2), the meteorological sensors and the SRA were operated to obtain simultaneous atmospheric and sea state data. The height H_{min} of the triangular flight pattern in (1) was as close to the sea surface as possible, depending on the weather conditions. It was designed to allow measurement and subsequent comparison of the wind stress behavior in the upwind/downwind and crosswind directions. The flight path in (2) at $2H_{min}$ was included to allow a comparison with measurements taken at a different elevation. Each track in (1) and (2) comprised a 20-min constant heading flight. It should be noted that the flight track direction on crosswind legs was different from the aircraft heading because of the wind drift, and the aircraft headings of both cross wind legs were nearly at 90° to the wind direction.

The mss was also acquired during the circle flight paths at about 240-m altitude at the beginning and the end of the atmospheric measurements. During circle flights, the aircraft was in a 7° roll attitude, with the SRA scanning from −15° to 29°, turning azimuthally through more than 720° to map the azimuthal dependence of the backscattered power falloff. These circle flight data will be reported elsewhere. The SRA was operated during level flight segments whenever the aircraft altitude was above the SRA 35-m minimum altitude.

To characterize the dominant sea state, we determined two-dimensional directional frequency spectra for each flight mission. For these determinations, the SRA was operated at the height of 1200 m for about 12 minutes. Here we present only the results, as details of the data processing methodology are described fully by Walsh et al. (1985).

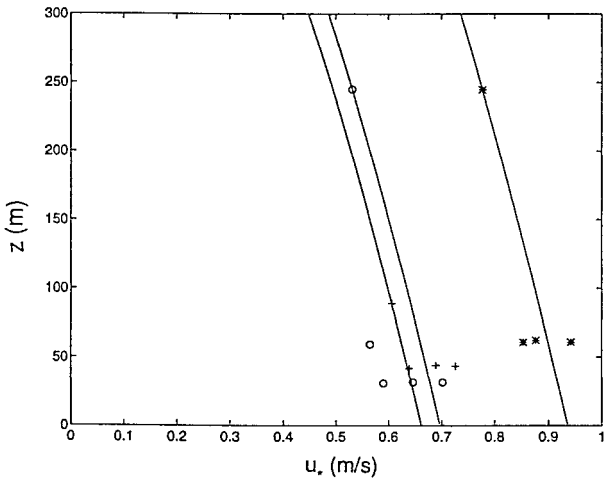

FIG. 6. Validation of surface stress correction (13): 10 June data (*), 11 June data (○), and 12 June data (+).

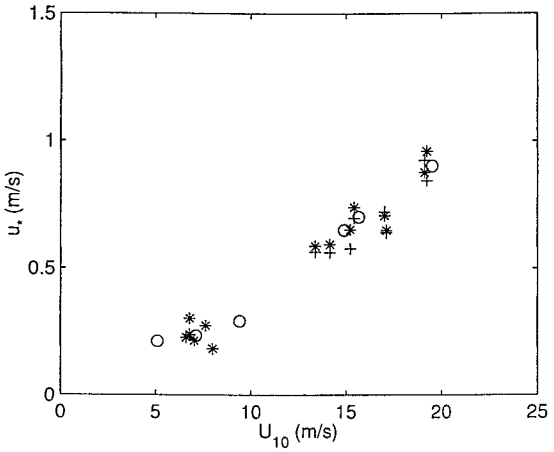

FIG. 7. Wind speed dependence of the friction velocity determined by the eddy-correlation method. Upwind/downwind flight data (*); crosswind flight data (○). Corresponding results at high wind speeds using the inertial-dissipation method are shown (+).

Vertical wind and temperature profiles through the MABL were recorded at the beginning and end of each flight mission through sounding flights from $H_{\min}$ up to a height of between 1300 and 2200 m. In addition to the laboratory instrument calibrations, in-flight calibrations were done on 14 and 18 June.

3. Mean results

In this paper we describe our methodology for calculating the drag coefficient and present the results obtained for the observed mean properties of the wind speed, wind stress, and sea state. A detailed discussion of their variability is described in a companion paper by Chen et al., Part II.

From the entire dataset, 29 subsets were selected for analysis to extract the mean atmospheric features. These comprised the measurements from the triangular flight tracks at $H_{\min}$ and the straight flight track at $2H_{\min}$ for each mission. In SOWEX, a suite of pressure and temperature sensors installed on the F27 aircraft provided the necessary data. After checking the performance of each sensor, the actual pressures and temperatures for these 29 datasets were recovered from the raw sensor data using filtering techniques. The humidity was obtained from the recovered dry and wet temperatures. The wind velocities were calculated from recovered pressures, temperatures, and inertial navigation system (INS) data using the GUSTO routine based on the method of Lenschow (1986). The sea surface temperature was measured by a nadir-look Barnes PRT-5 radiometer. The mean wind stress vector at the flight altitude was estimated by the eddy-correlation method, that is, $\boldsymbol{\tau}(z) = -\rho\overline{\mathbf{u}w}$. In terms of its scalar components, the magnitude of the wind stress is given by $\tau = \rho[(\overline{uw})^2 + (\overline{vw})^2]^{1/2}$, and its angle θ to the mean wind is determined by $\theta = \tan^{-1}(\overline{vw}/\overline{uw})$. In these expressions, the overbar represents the mean value over a suitable averaging interval. This is a major issue underlying wind stress determinations and is discussed in detail in Part II. For the overall means, the typical averaging distance was of O(80 km).

It is known (e.g., Wyngaard 1973; Donelan 1990) that a systematic underestimate of the surface wind stress results from the constant stress layer assumption. The wind stress measured at a greater distance above the water surface must be corrected to obtain the surface wind stress by including the influence of the Coriolis force and horizontal pressure gradient. This correction indicates that the wind stress decays with height and finally vanishes at the top of the MABL, according to the following:

$$\tau/\rho = u_*^2\left(1 - \frac{\alpha_0 f_c z}{u_*}\right), \tag{13}$$

where f_c is the Coriolis parameter given by $f_c = 1.454 \times 10^{-4}$ sin(lat) rad s^{-1} and $\alpha_0 = V_{gs}/u_*$, where V_{gs} is the component of the geostrophic wind normal to the surface wind. Following Donelan (1990), we assumed $\alpha_0 = 12$. Figure 6 provides a graph of this correction. The agreement of the superimposed SOWEX data at different altitudes supports the use of the above extrapolation to obtain the surface wind stress. The friction velocity extrapolated in this way from measurements made at different heights below 100 m is plotted against the neutral 10 m wind speed in Fig. 7. It is noted that, during SOWEX, the thermal stratification was unstable and, as is customary, the results were transformed to equivalent neutral stability conditions to allow convenient comparison of datasets obtained for different atmospheric stabilities. The conversion formula to obtain the drag coefficient C_{dn} from C_d is given by Panofsky and Dutton (1984) and Geernaert and Katsaros (1986):

$$C_{dn} = \left(C_d^{-1/2} + \frac{\psi_m}{\kappa} - \frac{1}{\kappa} \ln \frac{C_{dn}}{C_d} \right)^{-2}, \qquad (14)$$

where $C_d = u_*^2/U_{10}^2$, $C_{dn} = u_*^2/U_{10n}^2$ and U_{10n} is the neutral 10-m wind speed. Given U_{10} and the thermal stratification function ψ_m defined by (2), this may be solved iteratively for U_{10n}.

We also obtained estimates for u_* from the turbulence spectra (see Part II). We used the conventional value of the Kolmogorov constant of 0.52 and adjusted for the elevation and stability effects as for the eddy-correlation method above. These estimates are shown for the high wind speed days in Fig. 7 and are seen to agree closely with the eddy-correlation estimates.

With the above corrections, the mean atmospheric results for the 29 selected datasets are listed in Table 2. The neutral drag coefficient values for the range $5.1 < U_{10} < 19.5$ m s^{-1} have been calculated and are shown against the 10-m wind speed in Fig. 8. The mean linear regression of neutral drag coefficient values, determined from flights with altitudes less than 100 m and extrapolated to sea level, was

$$C_{dn} = (0.0713U_{10} + 0.7549) \times 10^{-3}, \qquad (15)$$

which is shown superimposed in Fig. 8a. The significant scatter in the drag coefficient results shown in this figure is in part due to the combination of variables presented in this plot, as the scatter in the companion Fig. 7 for u_* against U_{10} is significantly lower. For completeness, the corresponding variation of the coefficients of sensible and latent heat, C_h and C_e, with U_{10} are also shown in Fig. 8. These bulk aerodynamic coefficients and sensible and latent heat flux coefficients are defined and discussed in detail by Geernaert (1990). Reassuringly, these heat transfer coefficients observed in SOWEX have similar levels and lack of systematic wind speed dependence as reported in previous determinations.

An interesting finding during the gale force wind conditions in SOWEX concerns the aerodynamic roughness length z_0. Figure 9 shows z_0 plotted against the surface wind stress for the entire SOWEX period. We have chosen to examine the gale force wind days (10, 11, and 12 June) separately. A least squares best fit to the Charnock relationship (5) for these high wind speed data gave a coefficient $\alpha \sim 0.026 \pm 0.005$, as shown in Fig. 9. Comparison with previous datasets must be done carefully to exclude datasets involving shallow water and limited fetch observations (e.g., Garratt 1977; Wu 1980) which have reported generally higher α levels at a given wind speed. We have chosen to compare our results with Smith (1980) as these are more representative of unlimited fetch, open ocean conditions. This issue is taken up in the discussion (§4) below.

In SOWEX, the sea state was measured by the NASA SRA, shown schematically in Fig. 5. This unique instrument provided direct measurements of the large-scale sea surface topography, together with backscattered power level variation with off-nadir incidence angle. This allowed recovery of the directional wave spectrum for the dominant sea, as well as the mss. Directional wave spectra were determined from measurements made at a height of 1200 m and were processed using the methodology described by Walsh et al. (1985). Figures 10a–f show typical directional wave spectra during the SOWEX observational period. The associated significant wave heights and periods during the six experimental missions are given in Table 1. The gale force wind sea on 10 June shows spectral characteristics typical of a mature wind sea, with a narrow directional peak and increasing directional spreading toward higher frequencies. The form of the corresponding one-dimensional transect spectrum in the wind direction for the wind sea on 10 June is described subsequently.

During the upwind/downwind and crosswind track measurements, the SRA was operated to obtain simultaneous mss data with the wind speed and wind stress, as long as the flight altitude was sufficient to remain above the SRA minimum operating altitude limit (35 m). Such simultaneous mss data may be correlated with the wind speed, the wind stress, and the surface roughness length. The mss, however, is calculated from the properties of the SRA radar power reflected from the SRA, and its extraction is complicated and sensitive to many factors. Based on the model by Barrick (1968), the radar cross section per unit surface area σ is proportional to the joint probability density of the surface slopes $p(\zeta_x, \zeta_y)$ of the rough sea surface ζ; that is,

$$\sigma = \pi |R(0)|^2 \sec^4\theta \, p(\zeta_x, \zeta_y), \qquad (16)$$

where (ζ_x, ζ_y) are the slope components of the rough surface in two orthogonal directions, θ is the angle of incidence from the normal to the sea surface, and $R(0)$ is the Fresnel reflection coefficient of the surface at normal incidence. For an isotropic rough surface with Gaussian statistics, (16) becomes

$$\sigma_i = \frac{|R(0)|^2}{s^2} \sec^4\theta \exp(-\tan^2\theta/s^2), \qquad (17)$$

where s^2 is the total mss and the subscript i denotes an isotropic surface. By taking logarithms and using a Taylor series expansion in (17), for small incidence angles, we obtain

$$\begin{aligned} \ln\sigma_i &= \ln\frac{|R(0)|^2}{s^2} + \ln \sec^4\theta - \frac{\tan^2\theta}{s^2} \\ &= \ln\frac{|R(0)|^2}{s^2} + \left(2\theta^2 + \frac{1}{3}\theta^4\right) - \frac{\theta^2 + \frac{2}{3}\theta^4}{s^2} \\ &\quad + O(\theta^6). \end{aligned} \qquad (18)$$

We note that the derivative of the logarithm of the backscatter cross section with respect to the square of the incidence angle has an approximately linear relation with the reciprocal of the mss for nearly vertically incident radiation, since

TABLE 2. Summary of the mean results of the 29 selected datasets.

No	Date	Begin	End	Track	Dist (km)	z (m)	Dir	U_z	U_{10} (m/s)	u_* (m/s)	z_0 (mm)	C_d	C_h	C_e	H_s (m)	T_p (sec)	s^2
1	10	160205	161909	Upwind	78	63.03	235.5	23.02	19.50	0.902	1.762	2.141	0.93	0.88	9.2	13.6	0.0273
2	10	162045	163749	Crosswind	78	60.73	235.1	22.40	19.10	0.876	1.636	2.105	0.96	1.09	9.2	13.6	0.0386
3	10	164037	165741	Crosswind	78	58.22	239.3	22.72	19.22	0.959	3.306	2.491	1.11	0.89	9.2	13.6	0.0360
4	10	170050	171754	Crosswind	78	246.06	241.3	24.97	19.12	0.926	2.600	2.348	na	na	9.2	13.6	0.0346
5	11	131505	131921	Crosswind	19	250.60	250.0	15.81	11.90	0.684	9.487	3.303	na	na	4.2	12.1	0.0275
6	11	132358	133634	Crosswind	57	30.21	247.0	16.76	15.23	0.652	0.875	1.833	1.56	1.28	4.2	12.1	na
7	11	133735	135251	Upwind	69	29.71	243.9	17.24	15.67	0.702	1.328	2.008	1.22	1.02	4.2	12.1	na
8	11	135355	141001	Crosswind	73	29.90	243.9	15.48	14.15	0.594	0.733	1.765	1.37	1.08	4.2	12.1	na
9	11	141330	142843	Crosswind	69	59.28	250.8	15.39	13.37	0.587	1.097	1.925	1.22	1.66	4.2	12.1	0.0240
10	11	143129	144001	Crosswind	39	246.11	250.5	17.82	14.32	0.674	2.030	2.213	na	na	4.2	12.1	0.0389
11	11	144109	144941	Upwind	39	246.09	248.8	17.49	15.55	0.453	0.011	0.848	na	na	4.2	12.1	0.0200
12	11	150530	151402	Upwind	39	251.61	245.2	19.31	15.30	0.612	0.454	1.600	na	na	4.2	12.1	na
13	12	145700	151404	Crosswind	78	43.90	232.7	19.28	17.02	0.707	0.659	1.726	na	na	6.2	13.3	na
14	12	151602	153059	Upwind	68	43.62	234.0	16.83	14.91	0.650	1.035	1.900	na	na	6.2	13.3	0.0179
15	12	153408	154909	Crosswind	68	41.68	228.0	17.70	15.43	0.740	2.388	2.300	na	na	6.2	13.3	0.0295
16	12	155048	160719	Crosswind	75	88.94	229.4	19.78	17.12	0.649	0.260	1.436	na	na	6.2	13.3	0.0290
17	13	125817	131521	Upwind	78	31.41	203.1	9.98	9.41	0.292	0.025	0.963	1.07	na	4.0	13.8	na
18	13	131822	132654	Crosswind	39	35.16	200.9	8.29	7.99	0.183	na	0.527	na	na	4.0	13.8	na
19	13	132802	134348	Crosswind	72	33.24	193.2	8.17	7.63	0.274	0.142	1.284	1.41	na	4.0	13.8	na
20	13	134527	135359	Upwind	39	30.83	205.1	7.52	7.11	0.235	0.056	1.095	0.83	na	4.0	13.8	na
21	13	135557	141301	Crosswind	78	59.16	207.7	7.34	6.79	0.239	0.115	1.237	1.23	na	4.0	13.8	0.0125
22	14	133302	134536	Upwind	57	18.57	198.1	5.29	5.10	0.213	0.681	1.738	1.29	na	2.0	13.8	na
23	14	134817	135960	Crosswind	53	20.14	192.7	6.86	6.61	0.228	0.090	1.185	0.95	na	2.0	13.8	na
24	14	140252	142548	Crosswind	105	19.47	214.8	7.26	7.03	0.215	0.021	0.937	0.63	na	2.0	13.8	na
25	14	142732	144436	Crosswind	78	38.22	224.3	7.46	6.79	0.303	1.268	1.987	1.32	na	2.0	13.8	0.0135
26	16	150351	151758	Crosswind	64	19.40	204.1	1.48	1.33	0.873	na	na	0.98	0.82	1.0	9.8	na
27	16	151940	153003	Upwind	47	18.89	204.6	1.81	1.67	0.123	na	na	na	na	1.0	9.8	na
28	16	153125	154742	Crosswind	74	16.07	216.7	1.17	1.13	2.113	na	na	na	na	1.0	9.8	na
29	16	154840	160906	Crosswind	93	35.87	315.7	2.30	2.07	0.124	na	na	1.39	0.77	1.0	9.8	na

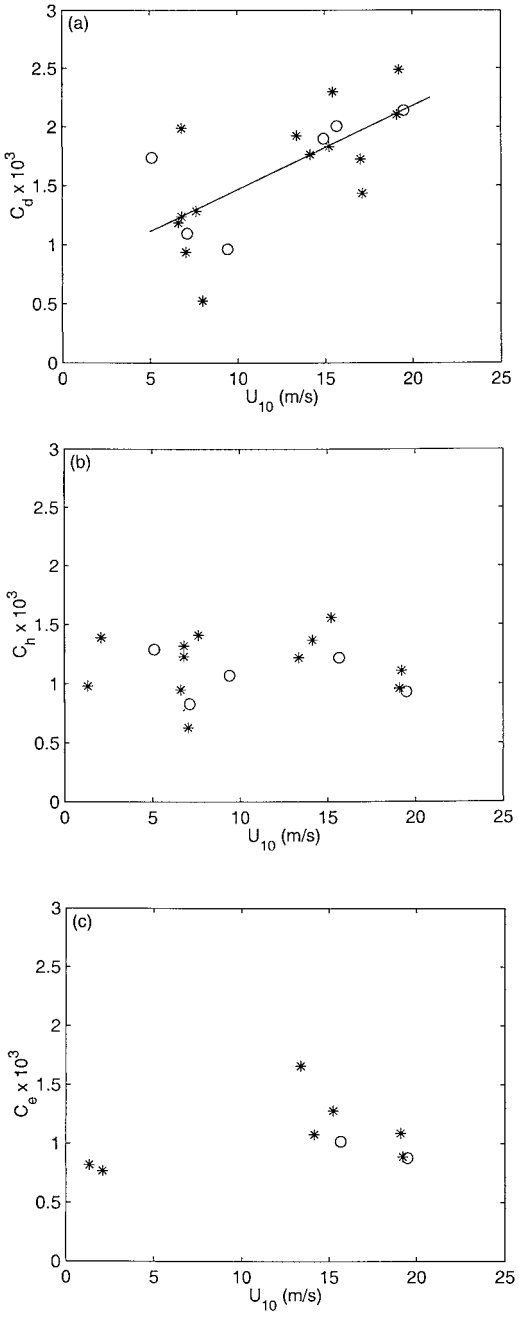

FIG. 8. Nondimensional coefficients for (a) momentum flux, (b) sensible heat flux, and (c) latent heat flux against neutral 10-m wind speed during SOWEX. Upwind/downwind flight data (*); crosswind flight data (○).

$$\frac{d\ \ln\sigma_i}{d\theta^2} \approx 2 - \frac{1}{s^2}. \tag{19}$$

For a more general, nonisotropic Gaussian rough surface, (17) becomes, for crosswind flight measurements (Valenzuela 1978),

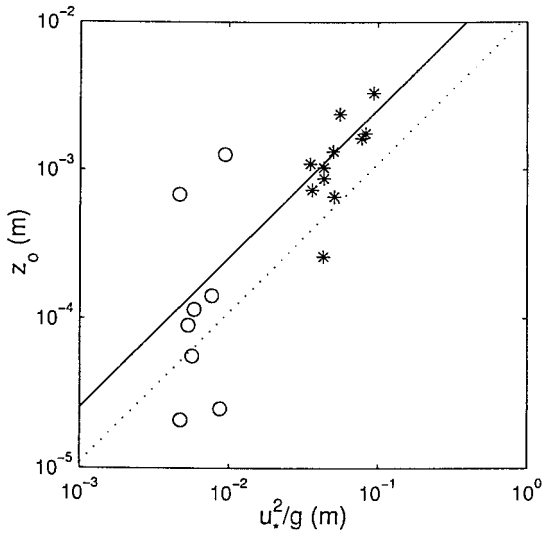

FIG. 9. Plot of roughness length z_0 against u_*^2/g for the SOWEX dataset, corrected to neutral stability. The results from high (>9 m s^{-1}) and low wind speeds are shown "*" and "○." The least squares best-fit solid line for the high wind speed data (*) has a Charnock coefficient $\alpha = 0.026 \pm 0.005$. The dotted line shows the value of $\alpha = 0.011$ reported by Smith (1980) for long fetch open-ocean conditions.

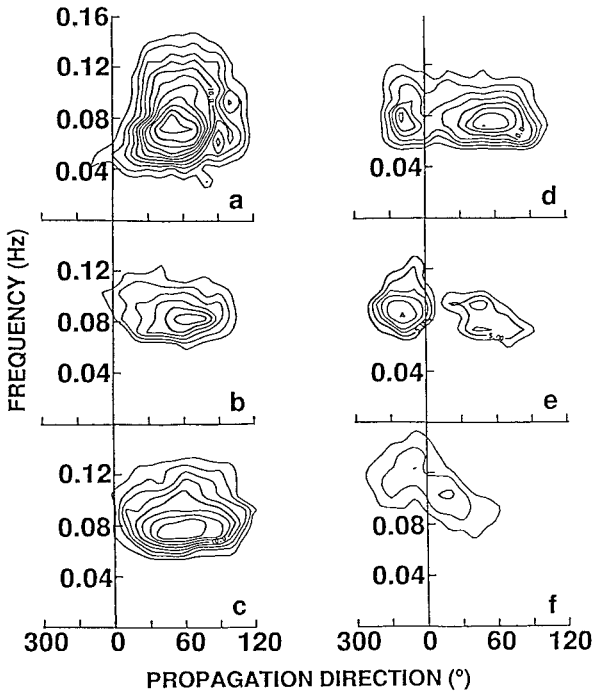

FIG. 10. Representative directional frequency spectra from the SRA data at 1200-m altitude on the various flight days (a) 10 June ($U_{10} \sim 20$ m s^{-1} from 323°), (b) 11 June ($U_{10} \sim 15$ m s^{-1} from 333°), (c) 12 June ($U_{10} \sim 16$ m s^{-1} from 310°), (d) 13 June ($U_{10} \sim 8$ m s^{-1} from 340°), (e) 14 June ($U_{10} \sim 7$ m s^{-1} from 340°), and (f) June 16 ($U_{10} < 2$ m s^{-1}, variable directionality).

$$\sigma_{niu} = \frac{|R(0)|^2}{2s_u s_c} \sec^4\theta \exp(-\tan^2\theta/2s_u^2), \qquad (20)$$

where s_u^2 and s_c^2 are respectively the mss components of the upwind and crosswind directions with $s^2 = s_u^2 + s_c^2$, and the subscript ni*u* denotes the upwind direction of a nonisotropic, rough surface. The backscatter cross-sectional falloff relation (19) becomes

$$\frac{d\ \ln\sigma_{niu}}{d(\theta^2)} \approx 2 - \frac{1}{2s_u^2}. \qquad (21)$$

Similarly, for upwind/downwind flight measurements, the backscatter cross-sectional falloff is

$$\frac{d\ \ln\sigma_{nic}}{d(\theta^2)} \approx 2 - \frac{1}{2s_c^2}, \qquad (22)$$

where the subscript ni*c* denotes the crosswind direction of a nonisotropic rough surface.

The incidence angle in (19), (21), and (22) is the angle of the beam with respect to the *local* mean normal to the sea surface. Consequently, before the linear regression was implemented in accordance with (21) or (22), the incidence angle of each beam was corrected, taking into account the aircraft attitude and the local mean sea surface tilt. This surface tilt correction for the incidence angle was needed as we found that the derived mss was sensitive to the tilt correction. This was also noted by Gotwols and Thompson (1994) in their ocean tower radar experiment. Because of noise in the raw SRA topography, it was necessary to apply filtering in order to reconstruct the sea surface topography as reliably as possible to determine the mean tilts. Figures 11a and 11b show typical raw sea surface elevation profiles in the wind direction measured during upwind/downwind and crosswind flight tracks respectively. The corresponding one-dimensional wavenumber transect spectra of the raw elevation data in the wind direction is shown in Fig. 11c. This plot indicates that the noise level in the crosswind direction is excessive, so we applied a two-sided, low-pass Butterworth filter to the elevations in each scan line to smooth the elevation profile noise. Sufficient filtering was used to correct the sea surface topography to conform to the k^{-3} form reported by Banner et al. (1989) and the resultant one-dimensional wavenumber transect spectrum is shown in Fig. 11d.

A linear best-fit regression to the backscatter cross-sectional falloff as plotted according to (21) and (22) is only valid over a limited range of incidence angles, which depends on the strength of the wind and the noise floor. Therefore, an incidence angle limit must be specified for the linear regression. For the strong wind days of 10, 11, and 12 June, this incidence angle limit is $\pm 15°$, as suggested by Barrick (1968). For the weak wind day of 13 June, the incidence angle should be limited to $\pm 12°$. This aspect is illustrated in Fig. 12e.

Due to the anisotropy of the sea surface roughness,

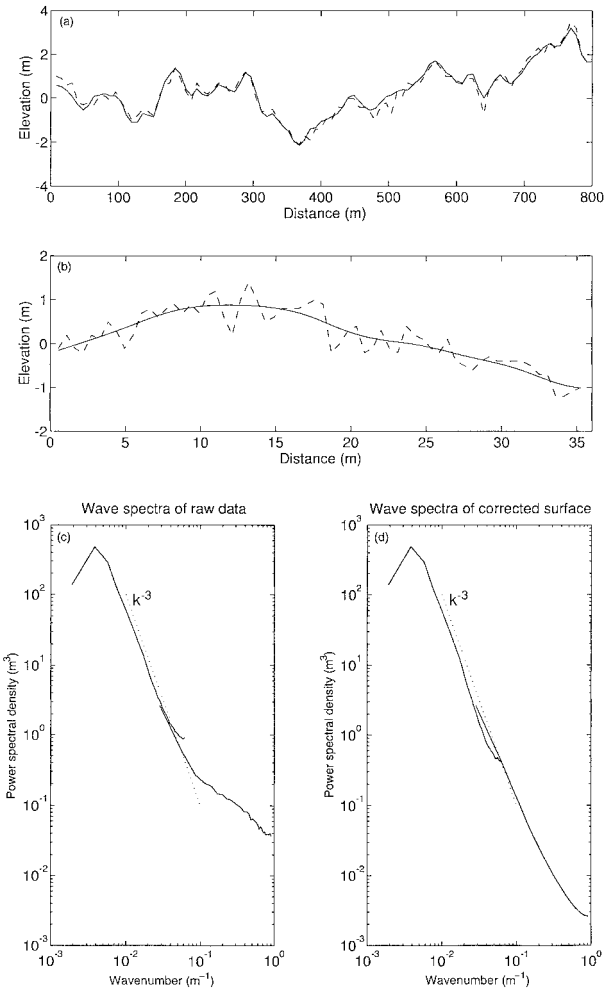

FIG. 11. (a) and (b) Typical SRA surface profile data in the wind direction measured during upwind/downwind and crosswind flight tracks, respectively. The dashed lines connect the actual data points; the solid lines are smoothed profiles. The degree of low-pass filtering was determined by the requirement for their transect spectra to have a k^{-3} dependence. (c) and (d) The transect spectrum for 10 June in the wind direction calculated from the raw and smoothed topography data, respectively. The high and low wavenumber sections were obtained from the crosswind and upwind/downwind SRA measurements, respectively.

only s_u^2 or s_c^2 may be determined from a given flight track, depending on the flight track orientation with respect to the wind. In Table 2, s_u^2 is given by crosswind flights and s_c^2 is given by upwind/downwind flights. These mss results are plotted against the 10-m wind speed in Fig. 13. The regressions for s_u^2 and s_c^2 are, respectively,

$$s_u^2 = 0.0019U_{10} \qquad (23)$$

and

$$s_c^2 = 0.0013U_{10} \qquad (24)$$

under the assumption that the mss is zero when wind

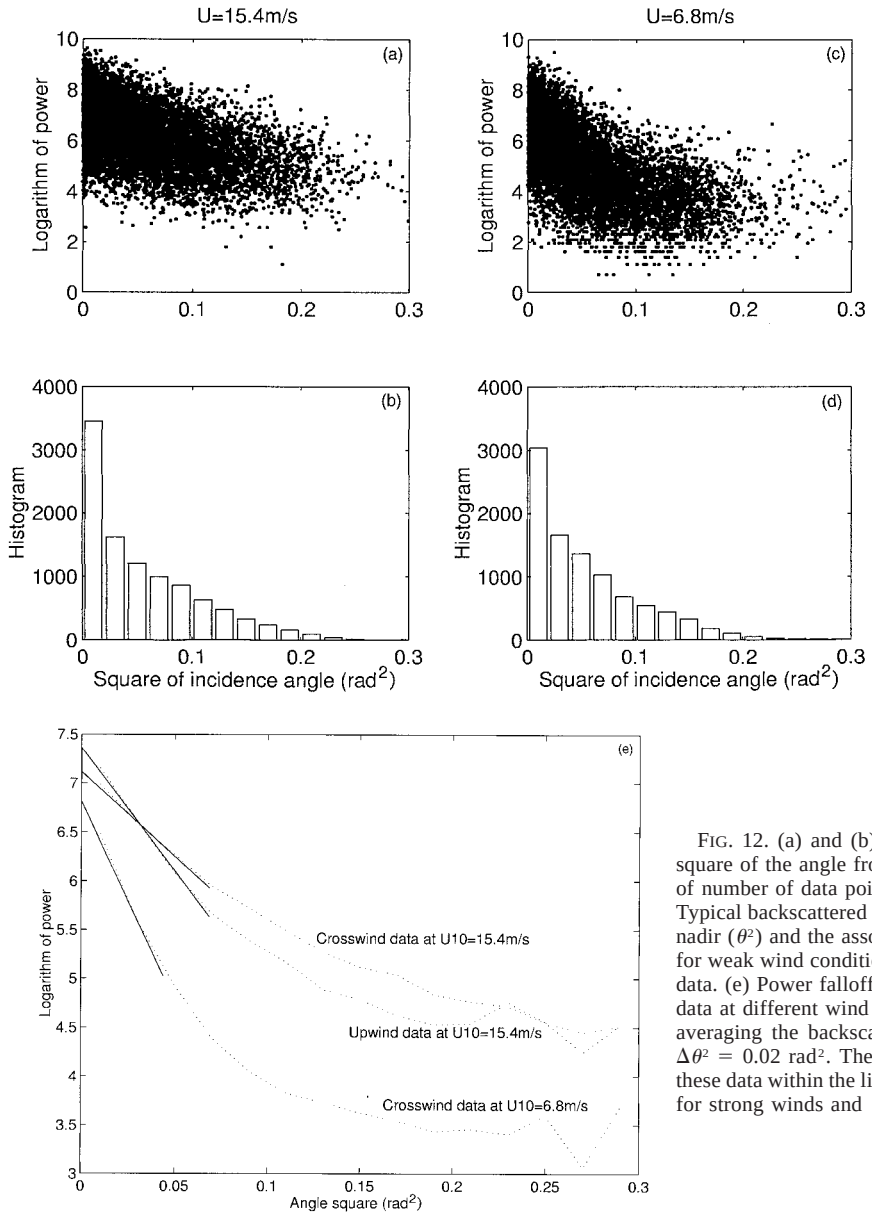

FIG. 12. (a) and (b) Typical backscattered power falloff with square of the angle from nadir (θ^2) and the associated histogram of number of data points for strong wind conditions. (c) and (d) Typical backscattered power falloff with square of the angle from nadir (θ^2) and the associated histogram of number of data points for weak wind conditions. Each dataset is from 200 lines of SRA data. (e) Power falloff with θ^2 comparing upwind and crosswind data at different wind speeds. The dotted lines were obtained by averaging the backscattered power data within angular bins of $\Delta\theta^2 = 0.02$ rad^2. The solid lines show the linear regressions of these data within the limited angular ranges about nadir, i.e., $\pm 15°$ for strong winds and $\pm 12°$ for weak winds.

speed is zero. Thus, the variation of total mss with U_{10} is

$$s^2 = s_u^2 + s_c^2 = 0.0032U_{10}. \quad (25)$$

In comparison with the previous studies, the mss levels obtained in SOWEX are about 0.6 times the levels reported by Cox and Munk (1954) and are comparable with the levels reported by Jackson et al. (1992) for strong wind conditions. The appreciable difference in mss levels reported by optical and radar methods is due primarily to the different measurement wavenumber bandwidths of these observations in relation to the capillary–gravity region of the wavenumber spectrum. According to the estimates of Jackson et al. (1992), diffraction limit effects cause an effective cutoff wavenumber corresponding to two to four times the SRA radar wavelength (8 mm).

It should be noted that we decided not to plot mss against u_* for several reasons, including the lower scatter inherent in our measurements of the mean wind speed. This issue is taken up at greater length in Part II.

Correlations of wind stress with sea state parameters

Wind sea conditions were not realized during SOWEX except on the first day (10 June) as discussed in section 2, hence there was very limited opportunity to

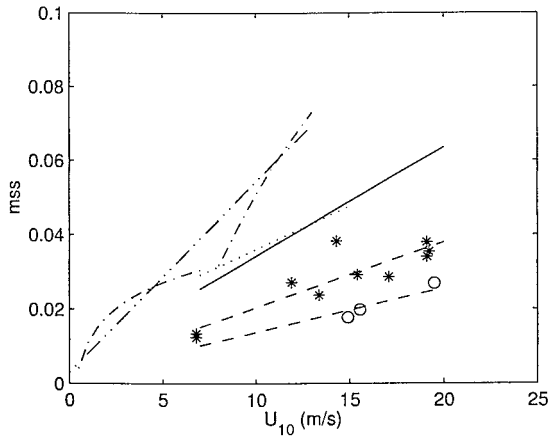

FIG. 13. Mean mss results from the 36-GHz SRA data plotted against the wind speed. The upwind/downwind and crosswind mss components are indicated by "*" and "○," respectively. The superposed lines are least squares best fit to the data (dashed). A data point at the origin was assumed for the crosswind slope; sum of the lines of best fit to data for the two slope components (solid); mss reported by Jackson et al. (1992) (dotted); linear fit proposed by Cox and Munk (1954) (double dot–dashed); two branch log-linear fit [Eq. (26)] proposed by Wu (1990) (dashed–dashed).

examine the validity of Donelan's generalization (8) of the Charnock relation (5). The relevant data for the gale force wind sea case on 10 June were used to compute the mean value of z_0/σ for the observed mean value of U_{10}/c_p. We found that (8) underpredicted the observed mean value of z_0/σ by a factor of $O(2)$. However, the agreement improved to within 25% and 10%, respectively, when u_* or $U(\lambda/2)$ was chosen for the reference velocity in conjunction with the appropriate coefficients A_0 and B_0 given in Table II of Donelan (1990). We also examined how these limited SOWEX wind sea data fitted the further refinement (12) of the Charnock relation proposed recently by Anctil and Donelan (1996). Since (12) is sensitive to the bandwidth of the mss measurement, a reduction factor was applied to the measured SOWEX mss levels (25-mm cutoff wavelength) to bring them to the same bandwidth (480-mm cutoff wavelength) on which (12) was based. This factor (0.54) was estimated from a high wavenumber wind wave spectral model. For the SOWEX wind sea data on 10 June, observed values of z_0/σ and values calculated from (12) agreed within 10%. Clearly, further wind sea studies over a wider range of wind speeds and wave ages that report mss are needed to explore this promising correlation. However, to evaluate its applicability to laboratory wind waves, as Donelan (1990) reported for (8), the bandwidth limitation imposed by the field mss values used in (12) will first need to be addressed.

4. Discussion

Within the SOWEX observational period, we successfully measured the wind stress and the sea surface roughness over a wide range of wind speeds from gale force to light and variable winds. Our major focus was on the stronger wind cases during which weakly unstable thermal stratification conditions and mature seas prevailed.

a. Exchange coefficients

SOWEX has made a significant contribution to the relatively sparse dataset available on the very high wind speed behavior of the standard exchange coefficients of momentum (C_d), sensible heat (C_h), and latent heat (C_e). In common with the recently published study by Yelland and Taylor (1996), the associated sea state conditions embracing large wave heights and extremely long wavelengths make this dataset distinctive. For the most part, the observed wind speed dependence of the exchange coefficients conform to those reported by previous authors.

We did observe an interesting feature of the nondimensional aerodynamic roughness length, or Charnock coefficient. For the high wind speed conditions ($13 < U_{10} < 20$ m s^{-1}) encountered during SOWEX, we found a Charnock coefficient of 0.026. This is significantly higher than values reported in previous investigations for unlimited fetch, open ocean conditions. For example, using $\kappa = 0.40$, Smith (1980) reported $\alpha \sim 0.01$ from his unlimited fetch, open ocean dataset spanning a wide range of wind speeds from 6 to 22 m s^{-1}. However, it is evident from his Fig. 6a that his choice of $\alpha \sim 0.01$ underpredicts his observed C_d regression at higher wind speeds. This point was also highlighted in section 4b(3) and Fig. 10 in the recent study by Yelland and Taylor (1996). Their very substantial open ocean dataset indicates that a significantly higher value of α is needed to fit their neutrally corrected C_d against U_{10} data for $15 < U_{10} < 25$ m s^{-1} than for $7 < U_{10} < 14$ m s^{-1}. However, it remains to be explained why their proposed high wind speed level of $\alpha \sim 0.017$ is somewhat lower than our SOWEX estimate for a similar wind speed range. This may be due to the very limited range of sea state conditions encountered during SOWEX compared with Yelland and Taylor (1996), but we were unable to pursue this further. We were also unable to investigate the possible relationship between the roughness length and the wave age.

The augmented Charnock coefficient α that is observed for higher wind speed ranges for nominally fully developed wind seas is noteworthy and has a possible explanation. Notwithstanding any additional effects on the surface layer dynamics caused by surface tearing and spray, a higher value of α is consistent with the recent predictions of Banner and Peirson (1998) shown in Fig. 2, based on their study of the behavior of the tangential drag coefficient. According to these authors, the tangential drag coefficient was found to decrease almost linearly with wind speed, while the total drag coefficient increased with wind speed. Thus, the wave

form drag coefficient increased relative to the tangential stress coefficient, implying a greater aerodynamic roughness as the wind speed increases. As there is no known relationship between α and the relative proportions of tangential stress and wave form drag, the behavior of these drag coefficients cannot easily be translated into equivalent changes in α.

b. Mean square slope

The observed variation of mss with reference wind speed U_{10} up to gale force winds reaching 20 m s^{-1} represents a significant extension of the wind speed range previously available. The mss results obtained from different flight directions in gale force wind conditions indicate a distinct anisotropy in this measure of sea surface roughness. In particular, we found that the crosswind mss is about 0.7 of the upwind/downwind mss, which is comparable with the findings of Cox and Munk (1954) at lower wind speeds. Another noteworthy feature of the SOWEX mean mss results is the finding that the mss varies linearly with the wind speed. A linear dependence on wind speed was reported earlier by Cox and Munk (1954) for wind speeds up to 13 m s^{-1}. This dependence was also reported more recently by Hwang et al. (1996) for lighter winds up to 8 m s^{-1}, although their mss values appear to be significantly higher. Wu (1990) proposed a two-branch fit over the entire wind speed range $0 < U_{10} < 20$ m s^{-1}, with a break at $U_{10} = 7$ m s^{-1}. Contrary to our findings, Wu suggested that a better fit results for the higher wind speed range using the log–linear correlation

$$\text{mss} = [-8.4 + 6.0 \ln(U_{10})] \times 10^{-2}. \qquad (26)$$

Due to its importance in the closely related contexts of short wind wave dynamics and to sea surface radar backscatter signatures, it remains to be explain how the quasi-linear dependence of mss on the wind speed can be reconciled with the wind speed exponents above unity that have been reported for laboratory measurements of very high wavenumber components of wind wave spectra (e.g., Jähne and Riemer 1990) and also for radar backscatter from very short wind waves in the Bragg scattering regime over the ocean (e.g., Jones and Schroeder 1978). This issue is revisited in Part II, which presents our extensive results on the spatial variability of the wind forcing and its coupling to variations in the underlying sea surface roughness.

5. Conclusions

This paper describes the scope, methodology, and mean results obtained during SOWEX, which contributed a unique dataset comprising coupled meteorological and sea state data gathered from a research meteorological aircraft for gale force wind and associated large storm wave conditions. We have reported the variation with wind speed of the dimensionless coefficients associated with momentum flux and sensible and latent heat fluxes, together with the behavior of the mean square slope for these extreme wind seas. The wind stress data are in close agreement with recently published Southern Ocean ship-based data of Yelland and Taylor (1996). The SOWEX heat flux coefficients and mean-squared sea surface slope measurements closely follow the trend of results obtained for lower wind speeds. However, the nondimensional sea surface aerodynamic roughness length (Charnock coefficient) we observed for gale force wind speeds was significantly higher than the levels reported for lower wind speeds. This accords with a similar trend observed by Yelland and Taylor (1996) and is consistent with predictions on the partitioning of the wind stress into skin friction and form drag by Banner and Peirson (1998). A detailed description of the comprehensive SOWEX observations on the variability of the coupled air–sea interaction over scales of O(80 km) for such very strong wind forcing and unlimited fetch conditions is described in our companion paper, Part II.

Acknowledgments. The authors gratefully acknowledge the support provided for this project by the Australian Research Council, the National Science Foundation, the CSIRO Marine Laboratory, the CSIRO Office of Space Science and Applications, and the NASA Physical Oceanography Program. We also acknowledge the excellent technical support provided by Cecil Maher and David Parkin.

REFERENCES

Anctil, F., and M. A. Donelan, 1996: Air–water momentum flux observations over shoaling waves. *J. Phys. Oceanogr.,* **26,** 1344–1353.

Banner, M. L., and W. L. Peirson, 1998: Tangential stress beneath wind driven air–water interfaces. *J. Fluid Mech.,* **364,** 115–145.

——, I. S. F. Jones, and J. C. Trinder, 1989: Wavenumber spectra of short gravity waves. *J. Fluid Mech.,* **198,** 321–344.

Barrick, D. E., 1968: Roughness surface scattering based on the specular point theory. *IEEE Trans. Antennas Propagation,* **AP 16,** 449–454.

Charnock, H., 1955: Wind stress on a water surface. *Quart. J. Roy. Meteor. Soc.,* **81,** 639–640.

Chen, W., 1997: An observational study of the variability of the wind stress and sea surface roughness. Ph.D. thesis, The University of New South Wales, Sydney, Australia, 94 pp.

Cox, C., and W. Munk, 1954: Statistics of the sea surface derived from sun glitter. *J. Mar. Res.,* **13,** 198–227.

Donelan, M. A., 1982: The dependence of the aerodynamic drag coefficient on wave parameters. Preprints, *First Int. Conf. on Meteorology and Air–Sea Interaction of the Coastal Zones,* The Hague, the Netherlands, Amer. Meteor. Soc., 381–387.

——, 1990: Air–sea interaction. *The Sea,* Vol. 9, B. LeMehaute and D. Hanes, Eds., Wiley-Interscience, 239–292.

——, F. W. Dobson, S. D. Smith, and R. J. Anderson, 1993: On the dependence of sea surface roughness on wave development. *J. Phys. Oceanogr.,* **23,** 2143–2149.

Edson, J. B., C. W. Fairall, P. G. Mestayer, and S. E. Larsen, 1991: A study of the inertial-dissipation method for computing air–sea fluxes. *J. Geophys. Res.,* **96,** 10 689–10 711.

Etling, D., and R. A. Brown, 1993: Roll vortices in the planetary boundary layer: A review. *Bound.-Layer Meteor.,* **65,** 215–248.
Fairall, C. W., and S. E. Larsen, 1986: Inertial dissipation methods and turbulent fluxes at the air–sea interface. *Bound.-Layer Meteor.,* **34,** 287–301.
Garratt, J. R., 1977: Review of drag coefficients over oceans and continents. *Mon. Wea. Rev.,* **107,** 915–929.
Geernaert, G. L., 1990: Bulk parameterisations for the wind stress. *Surface Waves and Fluxes.* G. L. Geernaert and W. J. Plant, Eds., Kluwer Academic, 91–172.
——, 1991: Temporal and spatial variability of the wind stress vector. *Radar Scattering from Modulated Wind Waves,* G. A. Komen and W. A. Oost, Eds., Kluwer, 89–104.
——, and K. B. Katsaros, 1986: Incorporation of stratification effects on the oceanic roughness length in the derivation of the neutral drag coefficient. *J. Phys. Oceanogr.,* **16,** 1580–1584.
——, S. E. Larsen, and F. Hansen, 1987: Measurements of the wind stress, heat flux and turbulence statistics over the North Sea during storm condition. *J. Geophys. Res.,* **92,** 13 127–13 139.
Gotwols, B. L., and D. R. Thompson, 1994: Ocean microwave backscatter distributions. *J. Geophys. Res.,* **99,** 9741–9750.
Hasselmann, K., and Coauthors, 1973: Measurements of wind-wave growth and swell decay during the Joint North Sea Wave Project (JONSWAP) *Dtsch. Hydrogr. Z.,* **A8** (Suppl.), No. 12, 95 pp.
Hwang, P. A., S. Atakturk, M. A. Sletten, and D. B. Trizna, 1996: A study of the wavenumber spectra of short water waves in the ocean. *J. Phys. Oceanogr.,* **26,** 1266–1285.
Jackson, F. C., W. T. Walton, D. E. Hines, B. A. Walter, and C. Y. Peng. 1992: Sea surface mean square slope from K_u-band backscatter data. *J. Geophys. Res.,* **97,** 11 411–11 427.
Jähne, B., and K. S. Riemer, 1990: Two-dimensional wavenumber spectra of small-scale water surface waves. *J. Geophys. Res.,* **95,** 11 531–11 546.
Janssen, J. A. M., 1997: Does wind stress depend on sea-state or not? A statistical analysis of HEXMAX data. *Bound.-Layer Meteor.,* **83,** 479–503.
Jones, W. L., and L. C. Schroeder, 1978: Radar backscatter from the ocean: Dependence on surface friction velocity. *Bound.-Layer Meteor.,* **13,** 133–149.
Komen, G. J., L. Cavaleri, M. Donelan, K. Hasselmann, S. Hasselmann, and P. A. E. M. Janssen, 1994: *Dynamics and Modelling of Ocean Waves.* Cambridge University Press, 532 pp.
Large, W. G., and S. Pond, 1981: Open ocean momentum flux measurements in moderate to strong winds. *J. Phys. Oceanogr.,* **11,** 324–336.
Lenschow, D. H., 1986: Aircraft measurements in the boundary layer. *Probing the Atmospheric Boundary Layer,* D. H. Lenschow, Ed., Amer. Meteor. Soc., 39–55.
Oost, W. A., 1997: The KNMI HEXMAX stress data—Revisit. *Bound.-Layer Meteor.,* **86,** 447–468.
Panofsky, H. A., and J. A. Dutton, 1984: *Atmospheric Turbulence.* Academic Press, 119–155.
Paulson, C. A., 1970: The mathematical representation of wind speed and temperature profiles in the unstable atmospheric surface layer. *J. Appl. Meteor.,* **9,** 857–861.
Phillips, O. M., 1977: *The Dynamics of Upper Ocean.* Cambridge University Press, 336 pp
Plant, W. J., 1982: A relationship between wind stress and wave slope. *J. Geophys. Res.,* **87,** 1961–1967.
Rieder, K. F., 1997: Analysis of sea-surface drag parmeterization in open ocean conditions. *Bound.-Layer Meteor.,* **82,** 355–377.
——, and J. A. Smith, 1998: Removing wave effects from the wind stress vector. *J. Geophys. Res.,* **103,** 1363–1374.
Smith, S. D., 1980: Wind stress and heat flux over the ocean in gale force winds. *J. Phys. Oceanogr.,* **10,** 709–726.
——, 1988: Coefficients for sea surface wind stress, heat flux and wind profiles as a function of wind speed and temperature. *J. Geophys. Res.,* **93,** 15 467–15 472.
——, and Coauthors, 1992: Sea surface wind stress and drag coefficients: The HEXOS results. *Bound.-Layer Meteor.,* **60,** 109–142.
Stewart, R. W., 1974: The air–sea momentum exchange. *Bound.-Layer Meteor.,* **6,** 151–167.
Valenzuela, G. R., 1978: Theories for the interaction of electromagnetic and oceanic waves—A review. *Bound.-Layer Meteor.,* **13,** 61–85.
Walsh, E. J., D. W. Hancock, D. E. Hines, R. N. Swift, and J. F. Scott, 1985: Directional wave spectra measured with the Surface Contour Radar. *J. Phys. Oceanogr.,* **15,** 566–592.
——, D. Vandemark, C. A. Friehe, S. P. Burns, D. Khelif, R. N. Swift, and J. F. Scott, 1998a: Measuring sea surface mean square slope with a 36 GHz scanning radar altimeter. *J. Geophys. Res.,* **103**(C6), 12 587–12 601.
——, and Coauthors, 1998b: Observations of sea surface mean square slope under light wind during TOGA Coupled Ocean–Atmosphere Response Experiment. *J. Geophys. Res.,* **103**(C6), 12 603–12 612.
Wu, J., 1980: Wind-stress coefficient over the sea surface near neutral conditions—A revisit. *J. Phys. Oceanogr.,* **10,** 727–740.
——, 1990: Mean square slopes of the wind-disturbed water surface, their magnitude, directionality and composition. *Radio Sci.,* **25,** 37–48.
Wyngaard, J. C., 1973: On surface-layer turbulence. *Workshop on Micrometeorology,* D. A. Haugen, Ed. Amer. Meteor. Soc., 101–149.
Yelland, M., and P. K. Taylor, 1996: Wind stress measurements from the open ocean. *J. Phys. Oceanogr.,* **26,** 541–558.